A Fast Point Pattern Matching Algorithm for Robust Spatially Addressable Bead Encoding

Abhik Datta, Adams Wai-Kin Kong, Soumita Ghosh and Dieter Trau

***Abstract*—Bead encoding is a key problem central to all bead based microarrays. Recently a spatially addressable bead encoding technique has been developed ([1], [2]) that alleviates the need for costly hardware while still allowing high-throughput analysis. This paper proposes a pattern matching based scheme that extends this bead encoding technique's usability to uncontrolled environments. A novel affine invariant point pattern matching algorithm is developed to achieve this. The proposed algorithm uses local features to overcome the combinatorial explosion problem encountered in matching corrupted point patterns. The use of efficient data structures is emphasized to make the algorithm fast and scalable. The proposed scheme can decode bead identities in assays involving thousands of beads in a few seconds. Evaluation results using both real and simulated data are presented.**

I. Introduction

IN bead based microarrays the biochemical reactions of the assay take place on the surface of micrometer sized spherical beads coated with capture probes (such as antibodies or oligonucleotides). During the assay, target analyte molecules in the sample are captured by the probe molecules while fluorescent labeled detector molecules bind to the captured target analyte molecules. This causes the beads to light up under fluorescence with intensity proportional to the concentration of the target analyte. Microarrays containing thousands of such beads, where each bead captures a different target analyte allow massively parallel multiplexed analysis of biomolecules. However, the random assembly of beads in these microarrays means that to perform multiplexed assay each bead must encode the identity of the capture probe it carries.

The most common bead encoding strategy is to use color based markers such as fluorescent dyes [3] or photoluminescent nanoparticles [4] to label the beads. However, color based encoding schemes require costly flow cytometers to achieve reasonable multiplexing. Other bead encoding schemes embed tiny barcodes onto the beads [5]. These schemes require costly equipment for manufacturing as well as for decoding bead identities.

To overcome these problems Ng et al. [1] and Trau et al. [2] developed a *spatially addressable bead encoding* scheme for DNA microarrays, where the spatial location of a bead is used as its identifier. The approach was later also extended to antibody and enzyme microarrays by Zhu and Trau [6]. This paper re-formulates the *spatially addressable bead encoding* scheme as a point pattern matching problem. The proposed approach imposes fewer restrictions on the fluorescence signal (image) acquisition process and is better suited for practical use.

The rest of the paper is organized as follows: Section 2 discusses the robust spatially addressable bead encoding scheme, Section 3 reviews the current point pattern matching methods, Section 4 details the matching algorithm, Section 5 discusses the experiments and presents the evaluation results and Section 6 draws conclusions.

II. Robust Spatially Addressable Bead Encoding

In the *spatially addressable bead encoding* scheme, beads are deposited onto the microarray chip in batches, such that all beads in a batch carry the same capture probe. The batches are deposited sequentially and a bright field image of the chip (henceforth referred to as a deposition image) is acquired after each deposition. An automatic bead detection algorithm is used to extract the location (spatial coordinates) of the beads in the deposition images and a record is maintained of the capture probe associated with each bead location. A 3-plex deposition process is illustrated in the left column of Fig. 1.

After the assay, a fluorescence image (henceforth referred to as bioassay image) is acquired to quantify the concentration of the analytes. In [1], [2] and [6] the bioassay image is assumed to be acquired such that it is well-aligned with the deposition image. Hence, the locations of the beads in the bioassay image can be used to identify the probes associated with them.

In this paper, a more realistic scenario is considered where the bead chip is produced in a (possibly commercial) manufacturing facility separate from where the bioassay is performed. In such a situation, the bioassay image is a transformed version of the deposition image and the two images have to be aligned to decode the bead identities. This is illustrated in the right column of Fig. 1. This alignment problem is formulated as a point (bead) pattern matching problem.

Manuscript received July 30, 2013.

Abhik Datta is with the School of Computer Engineering, Nanyang Technological University, Singapore 639798 (e-mail: abhik1@e.ntu.edu.sg).

Adams Wai-Kin Kong is with the School of Computer Engineering, Nanyang Technological University, Singapore 639798 (e-mail: adamskong@ntu.edu.sg).

Soumita Ghosh is with Ayoxxa Living Health Technologies Pte. Ltd., Block E3A, #07-02, 7 Engineering Drive 1, Singapore 117576 (e-mail: soumita.ghosh@ayoxxa.com).

Dieter Trau is with the Department of Bioengineering and the Department of Chemical & Biomolecular Engineering, National University of Singapore, Singapore 117576 (e-mail: bietrau@nus.edu.sg).

978-1-4799-3163-7/13/$31.00 ©2013 IEEE

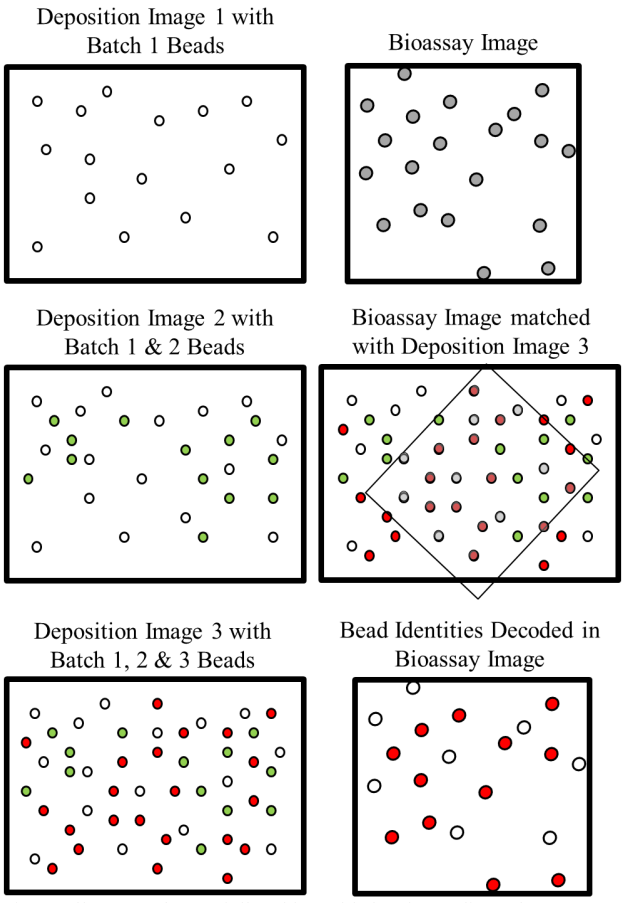

Fig. 1. Illustrates the spatially addressable bead encoding scheme.

The transformation between the deposition and bioassay image is affected by various factors, for instance the focal length (or zoom) of the imaging system and the orientation of the chip, when the bioassay image is acquired will determine the scale and rotation of the transformation respectively. Improperly calibrated equipment or dust can result in the chip not being leveled during bioassay image acquisition, introducing a small perspective distortion. To account for these an affine invariant matching algorithm is developed. Since the perspective distortion will be small, it can be locally approximated as affine.

Depending on the imaging system the bioassay image may only capture a small portion of the chip, because of limited field of view at the desired focal length. The matching algorithm therefore should be able to deal with occlusions. Contaminants can also pollute parts of the image and cause occlusion. Further, the bioassay image shows only those beads that produce a positive response. For instance in a 100-plex experiment if beads of only one of the batches produces a detectable positive response then 99% of the beads in the deposition image will not have a match in the bioassay image. Beads that do not have a match in the other image are considered as outliers. As the number of outliers increases the matching problem also becomes increasingly difficult. The proposed algorithm can find the correct match as long as at least 10-20% of the beads are inliers. To ensure that sufficient inlier beads are present in the bioassay image a batch of positive control beads is deposited as the first batch and the matching is done using the first deposition image.

III. Review of Point Pattern Matching Algorithms

Here we discuss the rigid point pattern matching algorithms most closely related to ours. Given the nature of our application and the problem, combinatorial matching algorithms are preferred over convex optimization based algorithms as the later are prone to get stuck in poor local minima. Spectral techniques are also ignored as they are highly sensitive to outliers and occlusions.

Geometric Hashing [7] is a model based registration framework which uses a hash table to perform the matching. The matching is achieved by evaluating the quality (or correspondences) of all the possible transformations. Pose Clustering [8] (also known as Generalized Hough Voting) is another popular combinatorial matching technique. It uses Hough voting to locate regions in the transformation space that are likely to contain the true transformation. For affine invariant matching however the number of possible transformations is a cubic function of the number of points in the set, consequently these methods are not scalable.

Random Sampling and Consensus (RANSAC) [9] is a parameter estimation technique that is widely used in computer vision. RANSAC iteratively generates transformation hypothesis and evaluates their quality. While it is capable of dealing with outliers, the number of iterations required to achieve a certain probability is inversely proportional to the number of outliers and occluded points. The number of iterations required for our problem makes the technique impractical.

Recently probabilistic graphical models based rigid point pattern matching algorithms [10], [11] have been developed where one of the point sets is represented as a rigid tree while the points in the other set are used as labels. Matching is achieved by maximizing the joint (tree) node-label assignment probability. They however, allow outliers in only one of the point sets. This cannot be guaranteed when automated bead detection algorithms are used to extract beads from the deposition and bioassay images.

Branch and bound (B&B) algorithms [12], [13] recursively sub-divide the search space into smaller sub-spaces and calculate lower bounds of the cost function in these sub-spaces. Only the sub-space with the lowest lower bounds on the cost function is further investigated. Genetic algorithm that searches the correspondence space [14] has also been developed for rigid point pattern matching. However, for larger point sets the correspondence space becomes too large even for B&B and Genetic algorithm based search.

Iterative techniques such as Iterative Closest Point (ICP) [15] have also found widespread success. ICP is however best suited when the transformation between the point sets is small.

Local affine invariants defined for four non-collinear points (we call them 4-points affine invariants or 4PAI) have also been widely used in computer vision [16], [17]. In [17], 4PAIs are used to register 3D surfaces. We use 4PAIs to match local patterns. However, our 4PAI extraction and matching is very different from that of [16] and [17].

IV. Bead Pattern Matching

Here, we assume that an automatic bead detection algorithm is used to detect beads in the deposition and bioassay images. The spatial coordinates of the beads extracted in such a way may have some positional errors, which are called jitter noise. We assume that the jitter noise follows a Gaussian distribution with a known standard deviation (σ_j).

Let $X_{2\times m} = [x_1, x_2, \dots, x_m]$, $x_i \in R^2$ be the spatial coordinates of beads detected in a bioassay image and $Y_{2\times n} = [y_1, y_2, \dots, y_n]$, $y_i \in R^2$ be the spatial coordinates of beads detected in a deposition image. Our objective is to find a binary correspondence matrix $P_{m\times n}$, whose element $p_{ij} = 1$ indicates that point x_i corresponds to point y_j.

Now if $m = n$ and P is an identity matrix, the relation between X and Y can be defined as:

$$Y_a = AX_a \tag{1}$$

where $Y_{a_{3\times n}} = \left[Y^T, 1_n{}^T\right]^T$, $X_{a_{3\times n}} = \left[X^T, 1_n{}^T\right]^T$, 1_n is an $n \times 1$ row vector with all 1s and $A = \begin{bmatrix} a_{11} & a_{12} & t_1 \\ a_{21} & a_{22} & t_2 \\ 0 & 0 & 1 \end{bmatrix}$ is a transformation matrix.

Therefore, given X and Y the affine transformation between them can be estimated through the least squares solution of the system:

$$AX_a - Y_a = 0 \tag{2}$$

i.e.,

$$\underset{A}{argmin}\ \ 1_n d((AX_a - Y_a)^T(AX_a - Y_a)) \tag{3}$$

where $d(M)$ is the column vector obtained using the diagonal elements of M.

In the matching problem however, the correspondences are not known and so we must evaluate and select a subset of all the possible correspondences. This objective can be defined as:

$$\underset{P,A}{argmin}\ \ 1_n d((AX_aP - Y_aP^T)^T(AX_aP - Y_aP^T)) \tag{4}$$

The general case where $m \neq n$ will be handled later. The optimization problem in equation 4 is hard because there are $n!$ possible permutation matrices, but given A, estimating P reduces to the well-known assignment problem [18]. Therefore the matching is done in two steps. First local patterns are matched to generate a set of candidate (or likely) estimates of A. These candidate As are further evaluated to find the best A. Then using the best A the assignment problem is solved to find the bead correspondences.

A. Sampling

Bioassay images can have thousands of beads. To reduce the complexity of the matching algorithm we use at most $m_s = \max(0.1n_b, 200)$ bioassay beads for matching, where n_b is the total number of beads used in the experiment. We assume that the beads are deposited following a uniform distribution, which is typical for most bead deposition mechanisms. Given m uniformly distributed beads the area (a_s) that will contain m_s beads is calculated and all the beads found in a central region of the image with area a_s are extracted as sample beads. If the bioassay image has fewer than m_s beads, all the beads are used as samples.

Notice that the number of beads in the bioassay image may be fewer than n_b, for instance when all the batches do not produce a positive response. Nevertheless, as long as the total number of positive control beads used (n_c) is large, we expect to find sufficient positive control beads for matching within the m_s sampled beads. If all the batches produce positive responses, the expected number of control beads within the sample will be $0.1n_c$, and in all other cases we will have greater than $0.1n_c$ control beads among the m_s sampled beads. Let $X^+{}_{2\times m_s}$ be the spatial coordinates of the sampled beads.

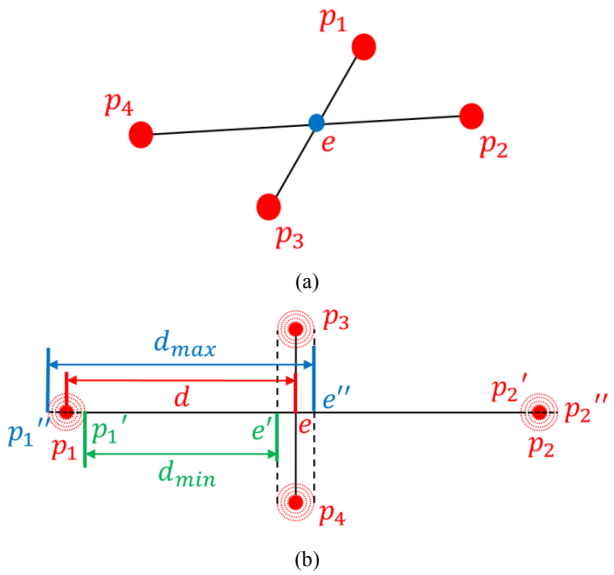

Fig. 2. (a) Shows two non-consecutive intersecting lines created from 4 points. (b) Illustrates the ratio range calculation for soft matching of 4PAI features.

B. Local Feature Extraction

Given four non-collinear points on a plane such that none of the points lie within the triangle formed by the remaining three points, it is always possible to form a pair of intersecting non-consecutive line segments by joining the points. An example is shown in figure 2(a).

Using the point of intersection e of the line segments p_1p_3 and p_2p_4 (see figure 2(a)) we calculate two ratios $r_1 = \frac{p_1e}{p_3e}$ and $r_2 = \frac{p_2e}{p_4e}$. Under affine transformation, the ratio of distances between co-linear points is preserved. Therefore the ratios r_1 and r_2 are affine invariant. These ratios form a descriptor for the pattern formed by p_1, p_2, p_3, and p_4. We

call this descriptor the 4-points affine invariant (4PAI) feature. By convention we calculate the ratios as $r_1 = \frac{\max(p_1e, p_3e)}{\min(p_1e, p_3e)}$ and $r_2 = \frac{\max(p_2e, p_4e)}{\min(p_2e, p_4e)}$.

To extract 4PAI features from a set of beads, lines are formed by joining each bead to its k nearest neighbor beads. To detect all the intersections among the L lines thus formed we use the Bentley-Ottman algorithm [19]. While a naive evaluation of intersections among L line segments takes $O\left(\frac{L(L-1)}{2}\right)$ time, the Bentley-Ottman algorithm takes $O((L + n_i)\log L)$ time, where n_i is the number of intersections found. Each line segment intersection found is used to generate a 4PAI feature.

4PAI features are extracted from both the sampled bioassay beads X^+ and deposition beads Y. The value of the parameter k depends on the amount outliers present in the set, and therefore different values (k_b and k_d) are used for the bioassay and deposition bead sets (respectively).

C. Local Feature Matching

The matching is done using a k-d tree constructed from the deposition 4PAI ratios. To account for jitter noise a soft matching is used, where for each bioassay 4PAI feature multiple approximately matched deposition 4PAIs are found.

Each bioassay 4PAI feature (r_1, r_2) is used to calculate an orthogonal matching range. To calculate this range, we assume that the actual bead lies within a distance of $3\sigma_j$ from its estimated position. Figure 2(b) illustrates the range calculation. To estimate bead location p_1 we assume that the actual bead lies within a circle of radius p_1p_1'. In the two extreme cases, the line segment p_1e can extend to $p_1''e''$ (d_{max}) or contract to $p_1'e'$ (d_{min}) and the ratio $r = \frac{p_1e}{p_2e}$ can become $r_{high} = \frac{p_1''e''}{p_2'e''} = \frac{p_1e+6\sigma_j}{p_2e-6\sigma_j}$ or $r_{low} = \frac{p_1'e'}{p_2''e'} = \frac{p_1e-6\sigma_j}{p_2e+6\sigma_j}$. For each bioassay 4PAI (r_1, r_2) we generate the orthogonal range as $\left(\left\{r_{1_{high}}, r_{1_{low}}\right\}, \left\{r_{2_{high}}, r_{2_{low}}\right\}\right)$ and find the approximately matching deposition 4PAIs by performing range query on the k-d tree. In R^2, orthogonal range queries can be performed using the k-d tree in $O\left(\log^2 n_{df} + c\right)$ time, where, n_{df} is the number of the deposition 4PAIs and c is the number of matches found.

D. Transformation Candidate Estimation

Each pair of matched deposition and bioassay 4PAI feature produces 4 correspondences, which is called an Approximate 4-Correspondences Set (A4CS). Given the four correspondences of an A4CS, equation 3 is used to calculate the affine transformation (we call this a candidate transformation) that best aligns (in a least squares sense) the corresponding points.

E. Candidate Transform Selection

Soft-matching of 4PAIs results in a large number of A4CSs, most of which are likely to be incorrect. Because solving the assignment problem to obtain the correspondence matrix P is costly, selection is performed to identify the best candidate transform.

True candidate transforms, i.e. candidate transforms generated from A4CSs containing true correspondences, will lie very close to each other in the transformation space. Moreover, when large k_b and k_d are used to calculate the 4PAIs, each bead participates in many 4PAIs and therefore many of them share the same inlier beads. Consequently many of the A4CSs containing true correspondences share the same correspondences. Thus a true candidate transform is likely to share correspondences with other true candidate transforms. These properties are used to select the optimal candidate transform.

Let $\hat{B}_{X^+{}_{2\times4}}$ be the quadrilateral obtained by applying a candidate transform A_c to the bounding box of X^+. A_c is represented as the $V_{1\times8}$ vector obtained by stacking together the rows of $\hat{B}_{X^+}$.

To rank the candidate transforms a *score* is calculate for each of them. Given a candidate transform V, other candidate transforms that lie within a distance of $6\sigma_j$ of V are identified using a k-d tree. Let n_r such neighbouring candidate transforms (V_i) are found. The *score* for V is then calculated as:

$$score = \frac{1 + \sum_{i=1}^{n_r} S_i}{\sum_{i=1}^{n_r} S_i \|V - V_i\|} \tag{5}$$

where $\|\cdot\|$ is the L_2-norm and

$$S_i = \begin{cases} 1, & if\ V\ and\ V_i\ share\ correspondence(s) \\ 0, & otherwise \end{cases} \tag{6}$$

A hash table is then used to check if the A4CS used to generate V and the A4CSs used to generate the neighboring transforms V_i share any correspondences. The top 200 candidate transforms with the highest *scores* are further evaluated to find the best candidate transform

To evaluate a candidate transform, the transformed bead coordinates $\hat{X}^+$ are generated from X^+. For each $x_i \in \hat{X}^+$, if there exists a $y_j \in Y$ such that $\|x_i - y_j\| < 6\sigma_j$ then $\{x_i, y_j\}$ is called a candidate correspondence. The search for candidate correspondences is also done using a k-d tree constructed from Y.

The candidate transform with the most x_is that have at least one candidate correspondence is determined as the best candidate transform.

F. Correspondence Estimation

The candidate correspondences found using the best candidate transform are then used to create a fuzzy correspondence matrix $F_{n_x \times n_y}$ whose elements

$$F(i,j) = \frac{1}{exp^{-\frac{(x_i - y_j)^T(x_i - y_j)}{2\sigma_j^2}}} \tag{7}$$

n_x and n_y are the number of x_i and y_j respectively, for which candidate correspondence(s) were found.

The fuzzy correspondence matrix F is reduced to a permutation matrix using the Hungarian algorithm [18]. When $n_x < n_y$, $(n_y - n_x)$ dummy rows with very high

correspondence costs are added to F. After the permutation matrix is found, the dummy rows and the columns corresponding to the dummy rows are discarded, producing a $n_x \times n_x$ permutation matrix. Given this permutation matrix, the optimal transformation A^* is estimated using equation 4. While the Hungarian algorithm requires $O({n_y}^3)$ time, each x_i produces few (in most cases 1) candidate correspondences, therefore there are few matching conflicts and the Hungarian algorithm requires only a few iterations.

To estimate the final bead correspondences (P^*), X is transformed by A^* and the same process of candidate correspondence estimation, fuzzy correspondence matrix generation and permutation matrix estimation are repeated using $\hat{X}$ and Y.

V. Experiments And Results

Our database consists of 148 deposition images and 202 bioassay images generated from a total of 56 experiments. The experiments ranged from 1-plex to 5-plex and were performed using polystyrene beads from different providers coupled to antibodies. The beads were deposited onto a 48 well biochip (Prokemion, Ayoxxa Living Health Technologies, Singapore) with a hexagonal grid of microwells in each well to capture the beads. The deposition images were obtained using a DSLR camera (EOS 5D Mark II, Canon, Japan) mounted on top of an infinity corrected objective lens (UIS2, Olympus, Singapore). The bioassay images were acquired using an epifluorescent microscope (BX41, Olympus, Singapore) with a digital CCD camera (Retiga-4000R, QImaging, Canada).

The proportion of incorrectly matched inlier bioassay beads or the Hamming error is used as the performance measure for all the tests. The algorithm was implemented in Matlab 8.0 and all the experiments were performed on a standard desktop computer with an Intel Quad Core 3 GHz processor and 4GB RAM.

To establish the ground truth matches, a few bead correspondences were detected through visual inspection of the bioassay-deposition image pairs. And the optimal transformation was estimated as the least median squares transformation that registered the detected correspondences.

Table 1 shows the matching performance for the 56 experiments. The number of beads used in each experiment ranged from approximately 300 to 800. For such small point sets and limited multiplex, the algorithm is able to find the correct transformation between the point sets in all cases (as shown in column 5 of Table 1). The small hamming error is due to a few bead correspondences that could not be established even under the correct transformation, possibly due to jitter noise. For this test k_b=10 and k_d=10 were used. All the batches (including the positive control batch) in these experiments have nearly the same size. Therefore, the percentage of positive control beads is $1/p$, where p is the number of batches (or multiplex). For this test σ_j was estimated using the ground truth correspondences of a subset of the dataset (10 deposition and 10 bioassay images).

TABLE I
Matching Results For Real Data

Multiplex	No. of Experiments	Mean Hamming Error (HE)	HE (Std. Dev.)	% Times HE > 0.5
1	24	0.001	0.003	0%
2	4	0.001	0.001	0%
3	4	0.003	0.004	0%
4	16	0.003	0.003	0%
5	8	0.003	0.006	0%

To rigorously establish the matching performance 9000 simulated experiments were performed. The simulated data was generated from 10 real deposition images. Gridding was performed on these deposition images to locate the hexagonal grid and identify the spatial coordinates of the microwells. All 10 deposition images had more than 50000 microwells. The simulated bead patterns were generated by randomly sampling microwells (i.e. microwell's spatial coordinates) from the grid.

For the simulated data, experiments of six different sizes (ranging from 500 to 5000 beads) and with three levels of positive control beads (10%, 15% and 20% of the total number of beads used in the experiment) were considered. Since the deposition image used for matching has only positive control beads, as the number of batches producing a positive response in the bioassay image increases so does the number of outliers. To test the robustness of the algorithm two levels of outliers were tested. The *average case*, where 50% of all the beads used in the experiment are present in the bioassay image and the *worst case* where all the beads are present in the bioassay image. For each of these 36 combinations (6 sizes, 3 levels of positive control beads and 2 levels of outliers) multiple simulations were performed and for each simulation, values of k_d and k_b ranging from 5 to 25 were tested. Table 2 shows the results for two pairs (k_d=10, k_b=15) and (k_d=10, k_b=25). To simulate jitter noise the bioassay beads were translated in a random direction by a distance d, where d is drawn from a Gaussian distribution with standard deviation $\sigma = 0.5d_n$ and d_n is the distance between neighboring microwells in the grid from which the bioassay pattern was generated.

When 20% positive control beads are present, accurate matching can be achieved in the *worst case*, using k_d=10 and k_b=15 (shown in boldface). When 15% positive control beads are present, matching using k_d=10 and k_b=25 is still sufficient to obtain correct matches in the *worst case* (shown with underlines). Once again the small Hamming error is due to a few bead correspondences that could not be established even when the correct transformation was found. The mean running times for the six different experiment sizes, using k_d=10 and k_b=15 are presented in Fig. 3. With n_b=5000 and n_c=1000 (20% positive control beads) matching takes around 90 seconds. With n_b=5000, at least 4000 beads are available for multiplexing which can be used to perform assays with hundreds of different probes.

TABLE II
MATCHING RESULTS FOR SIMULATED DATA

Total number of beads used in the experiment (n_b)		Mean Hamming Error (using k_d=10)											
		n_b=500		n_b=1000		n_b=2000		n_b=3000		n_b=4000		n_b=5000	
Number of positive control beads (n_c)	% of total beads present in bioassay image	k_b=15	k_b=25	k_b=15	k_b=25	k_b=15	k_b=25	k_b=15	k_b=25	k_b=15	k_b=25	k_b=15	k_b=25
n_c =10% of n_b	50%	0.017	0.005	0.002	0.001	0.002	0.001	0.007	0.001	0.005	0.003	0.052	0.012
n_c =10% of n_b	100%	0.111	0.014	0.149	0.011	0.105	0.001	0.191	0.005	0.257	0.018	0.576	0.190
n_c =15% of n_b	50%	0.001	0.001	0.001	0.001	0.001	0.001	0.001	0.001	0.001	0.001	0.001	0.001
n_c =15% of n_b	100%	0.007	0.002	0.001	0.001	0.001	0.001	0.001	0.001	0.001	0.001	0.063	0.001
n_c =20% of n_b	50%	0.001	0.001	0.001	0.001	0.001	0.001	0.002	0.001	0.001	0.001	0.001	0.001
n_c =20% of n_b	100%	**0.001**	0.001	**0.001**	0.001	**0.001**	0.001	**0.001**	0.001	**0.001**	0.001	**0.001**	0.001

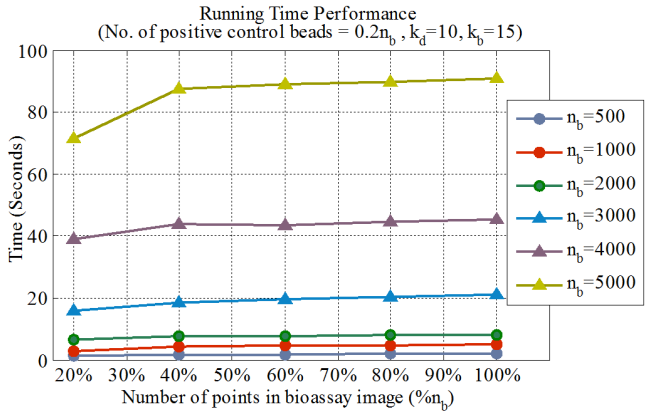

Fig. 3. Shows the time required to perform matching for various point sizes.

VI. CONCLUSIONS

A software based bead encoding technique is presented that uses the bead patterns formed in randomly assembled bead based microarrays to perform the encoding. Using the naturally formed bead patterns to identify the beads alleviates the need for any specially designed hardware. The proposed technique can be used to perform fast, high-throughput multiplex assays using any bead based biochip and with commonly available laboratory equipment such as a fluorescent microscope. The affine invariant matching algorithm developed to perform the encoding can handle large amounts of distortions and therefore places minimal constraints on the bioassay image acquisition process.

REFERENCES

[1] J. K. Ng, E. S. Selamat, and W.-T. Liu, "A spatially addressable bead-based biosensor for simple and rapid DNA detection," *Biosensors & Bioelectronics*, vol. 23, pp. 803-810, 2008.

[2] D. Trau, W.-T. Liu, and J. K. Ng, "A microarray system and a process for producing microarrays," WO0020080163335A1, February 7, 2008.

[3] K. L. Kellar and M. A. Iannone, "Multiplexed microsphere-based flow cytometric assays," *Expert Hematology*, vol. 30, no. 11, pp. 1227-37, Nov 2002.

[4] Y. Li, E. C. Y. Liu, N. Pickett, P. J. Skabara, S. S. Cummins, S. Ryley, A. J. Sutherland, and P. O'Brien, "Synthesis and characterisation of CdS quantum dots in polystyrene microbeads," *Journal of Material Chemistry*, vol. 15, pp. 1238-1243, 2005.

[5] R. Wilson, A. R. Cossins, and D. G. Spiller, "Encoded microcarriers for high-throughput multiplexed detection," *Angewandte Chemie-International Edition*, vol. 45, no. 37, pp. 6104-6117, 2006.

[6] Q. Zhu and D. Trau, "Multiplex Detection Platform for Tumor Markers and Glucose in Serum based on a Microfluidic Microparticle Array," *Analytica Chimica Acta*, vol. 751, pp. 146–154, November 2012.

[7] Y. Lamdan and H. J. Wolfson, "Geometric Hashing: A General And Efficient Model-based Recognition Scheme," in *Second International Conference on Computer Vision*, 1988.

[8] G. Stockman, "Object recognition and localization via pose clustering," *Computer Vision, Graphics, and Image Processing*, vol. 40, no. 3, pp. 361-387, 1987.

[9] M. A. Fischler and R. C. Bolles, "Random sample consensus: a paradigm for model fitting with applications to image analysis and automated cartography," *Communications of the ACM*, vol. 24, no. 6, pp. 381-395, 1981.

[10] J. J. McAuley, T. S. Caetano, and M. S. Barbosa, "Graph Rigidity, Cyclic Belief Propagation, and Point Pattern Matching," *IEEE Transactions on Pattern Analysis and Machine Intelligence*, vol. 30, no. 11, pp. 2047-2054, 2008.

[11] T. S. Caetano and J. J. McAuley, "Faster Graphical Models for Point-Pattern Matching," *Spatial Vision*, vol. 22, no. 5, pp. 443-53, 2009.

[12] D. P. Huttenlocher and W. J. Rucklidge, "A multi-resolution technique for comparing images using the Hausdorff distance," in *IEEE Computer Society Conference on Computer Vision and Pattern Recognition (CVPR)*, 1993, pp. 705-706.

[13] D. M. Mount, N. S. Netanyahu, and J. L. Moigne, "Efficient algorithms for robust feature matching," *Pattern Recognition*, vol. 32, no. 1, pp. 17–38, Jan 1999.

[14] N. Ansari, M.-H. Chen, and E. S. H. Hou, "Point pattern matching by a genetic algorithm," in *16th Annual Conference of IEEE Industrial Electronics Society*, 1990.

[15] P. J. Besl and N. D. McKay, "A method for registration of 3-D shapes," *IEEE Transactions on Pattern Analysis and Machine Intelligence*, vol. 14, no. 2, pp. 239-256, 1992.

[16] D. P. Huttenlocher, "Fast affine point matching: an output-sensitive method," in *IEEE Computer Society Conference on Computer Vision and Pattern Recognition* , 1991.

[17] D. Aiger, N. J. Mitra, and D. Cohen-Or, "4-points congruent sets for robust pairwise surface registration," *ACM Transactions on Graphics (TOG) - Proceedings of ACM SIGGRAPH*, vol. 27, no. 3, 2008.

[18] J. Munkres, "Algorithms for the Assignment and Transportation Problems," *Journal of the Society for Industrial and Applied Mathematics*, vol. 5, no. 1, pp. 32-38, 1957.

[19] J. L. Bentley and T. A Ottmann, "Algorithms for Reporting and Counting Geometric Intersections," *IEEE Transactions on Computers* , vol. C-28, no. 9, pp. 643-647, 1979.